Journal of Visualization, Vol. 2, No. 1 (1999) 37-50

Laser Holographic Observation of Cavitation Cloud on a Foil Section

Kato, H.*, Yamaguchi, H.*, Maeda, M.*, Kawanami, Y.* and Nakasumi, S.*

* Department of Environmental and Ocean Engineering, University of Tokyo, Tokyo, Japan.

Received 12 February 1999.
Revised 1 June 1999.

***Abstract*:** Observation of a cavitation cloud was performed using an off-axis laser holography system. The cavitation cloud contains an inverse U-shaped vortex cavitation surrounded by many small cavitation bubbles. The density of bubbles with radius larger than 35 μm is on the order of 10^3 bubbles/cm^3. The bubble number distribution was determined from the observation and by counting individual bubbles in reconstructed holographic images of the cavitation cloud.

***Keywords*:** cavitation, holography, bubble, cloud, foil.

1. Introduction

Cavitation is a vapor-liquid flow phenomenon with vaporization and condensation. Cavitation is very similar to boiling. The difference is that boiling is caused by superheating of the liquid, whereas cavitation is caused by an increase in the flow velocity resulting in a pressure lower than the vapor pressure. The vapor pressure of cold water is about 2.3 kPa at 20°C. If a cold water flow of 10 m/s under atmospheric pressure is accelerated to 20 m/s, the static pressure reaches a value well below the vapor pressure, resulting in the generation of cavitation in the flow. Cavitation occurs in any kind of fluid machinery, from a marine propeller to a liquid hydrogen feed pump of a space rocket. It causes a sudden drop in machine performance, severe noise and vibration, and finally destruction (erosion) of the machinery itself. Several books exist on the cavitation phenomenon (Knapp et al., 1970; Hammitt, 1980; Young, 1989; Brennen, 1995; Kato, 1996).

The inception of cavitation and its appearance are closely related to the characteristics of the boundary layer on a solid surface where cavitation might occur. Cavitation is usually classified as follows:

– Bubble cavitation
– Sheet cavitation
– Cloud cavitation
– Tip-vortex cavitation

Figure 1 shows the typical types of cavitation generated on a foil. When the boundary layer separates near the leading edge of the foil section, sheet cavitation occurs. On decreasing the static pressure, sheet cavitation grows and becomes increasingly unstable. Finally, the rear part of sheet cavitation is torn off and collapses downstream. This is called cloud cavitation by its appearance. Cloud cavitation is the most harmful type of cavitation because many small cavitation bubbles collapse simultaneously, generating a high pressure of more than 1 GPa in a very short time, much less than a millisecond. A cloud cavitation consists of many small cavitation bubbles (See Fig. 1 (c), which is sometimes called a "cavitation cloud."

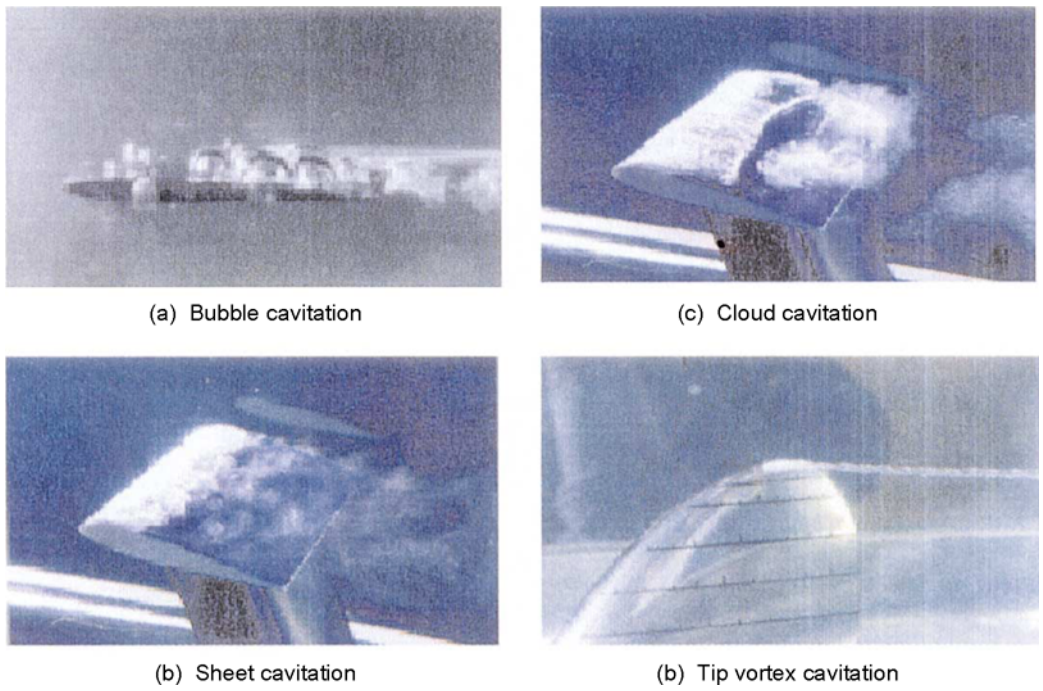

Fig. 1. Typical types of cavitation.

When the boundary layer does not separate, sheet cavitation never occurs, and instead, bubble cavitation occurs. Bubble cavitation is generated from tiny air bubbles in the flow. Tip-vortex cavitation is generated in the low-pressure zone of a vortex core.

Cloud cavitation was originally found by Knapp (1955), and has been investigated by many researchers, including Shen and Peterson (1978), Avellan et al. (1988), Kubota et al. (1989), de Lange et al. (1994), Reisman and Brennen (1996), and Kawanami et al. (1997, 1998). These researchers observed cloud cavitation using photography and/or high-speed cinematography (including high-speed video), and tried to elucidate the relationship between cavitation cloud behavior and detrimental effects such as severe noise and erosion.

Observation of air nuclei in water was initiated by Acosta et al. (1986) and Billet et al. (1986). They used inline holography which was simpler and easier than off-axis holography. Observation of a cavitation cloud by off-axis holography was made by Yamaguchi et al. (1990) and Maeda et al. (1991). Recently, Yu and Ceccio (1997) measured diffusion-induced bubble populations downstream of a small partial cavity. They used an in-line holograph system, and found the same tendency of bubble population as that in Maeda et al.'s measurement.

Theoretical analysis of cavitation clouds was initiated by van Wijngaarden (1964), who calculated the maximum pressure on a solid surface resulting from the one-dimensional collapse of a cavity cloud. Since then many scientists, such as Mϕrch (1981), Chahine (1983), Takahira et al. (1994), Wang and Brennen (1994), Brennen et al. (1998), and Matsumoto (1998) have analyzed the behavior of cavitation clouds. They all noted that the impulsive pressure increases very much due to the interaction between bubbles and shock waves.

Matsumoto (1998), for example, calculated the symmetric collapse of a spherical cavitation cloud. The calculated maximum impulsive pressure increases to more than ten thousand times the initial surrounding pressure, i.e., the maximum pressure reaches more than 1 GPa. Fortes-Patella and Reboud (1995) performed an erosion experiment using a Venturi-type facility and estimated an impulsive pressure as 2.5 GPa by analyzing the eroded pit shape. Konno et al. (1998) measured an impulsive force on the order of 10 N using a piezoelectric sensor. If we assume that the area of impulsive force is 100 μm in diameter, an impulsive pressure on the order of 1 GPa is calculated. Although the three results cannot be compared directly, it can be concluded that the collapse of a cavitation cloud generates a very high pressure impulse because of bubble/shock interaction, leading to severe erosion and noise.

In spite of theoretical and experimental studies, the fundamental knowledge regarding cavitation clouds is insufficient. The measurement of the instantaneous spatial distribution of cavity bubbles in a cavitation cloud is the most important for deeper understanding of cloud cavitation.

This paper reports on the observation of a cavitation cloud on a 2D foil section by off-axis holography,

including the measurement of cavity bubble number distributions, and is an extension of our previous researches (Yamaguchi et al., 1990; Maeda et al., 1991).

2. Experimental Setup and Cavitation Appearance

A two-dimensional (2D) foil, NACA 0015, was used for the present experiment. The chord length and span width were 80 mm and 150 mm, respectively. The foil section was installed in the Foil Test Section of the Marine Propeller Cavitation Tunnel at the University of Tokyo. The working section of the tunnel was rectangular, 600 mm in height and 150 mm in width. The 2D foil, both sides of which were softened by 10 mm-thick Teflon to preserve the highly accurate glass windows manufactured exclusively for the holography tests, was sustained by two struts connected to the bottom of the test section as shown in Fig. 2. The foil angle of attack was 8.4 deg. The uniform flow velocity and the water temperature were 8.0 m/s and 23-24°C respectively, resulting in the Reynolds number of 6.9×10^5. The air content ratio of the water measured by a dissolved oxygen meter was 10-15% of the saturated condition at 1 atm.

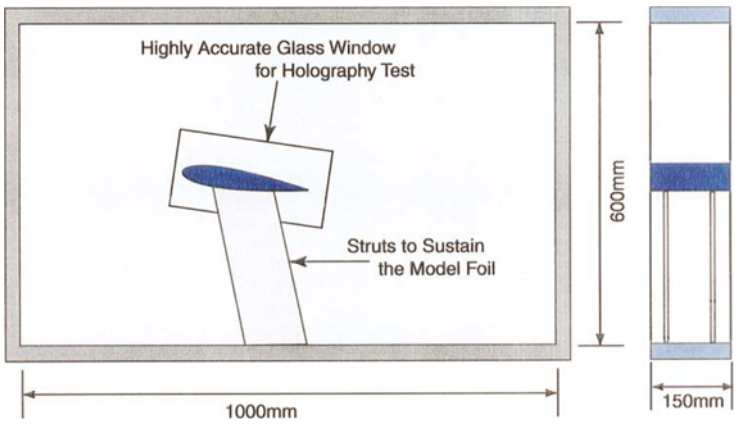

Fig. 2. Cavitation tunnel test section and model foil: Foil test section of marine propeller cavitation tunnel at the University of Tokyo and NACA0015.

The appearances of cavitation on the NACA 0015 foil are already shown in Figs. 1 (b) and (c). Those photographs were taken through large side windows (not through the optical windows shown in Fig. 2).

The cavitation condition is primarily governed by the cavitation number σ, defined as,

$$\sigma = \frac{p_\infty - p_s}{\frac{\rho}{2} U_\infty^2} \tag{1}$$

where p_∞: static pressure at infinity,
p_s: vapor pressure of water,
ρ : density of water,
and U_∞ : uniform velocity.

The sheet cavitation incepts at the leading edge of the foil first. With decreasing cavitation number, the sheet cavitation becomes longer and discharges a small cavitation cloud from its trailing edge, as seen in Fig. 1 (b). With a further decrease in cavitation number, the sheet cavitation becomes unstable and begins to periodically discharge a large cavitation cloud.

This cavitation cloud is an inverse U shape and its two legs are attached to the foil surface. According to Kubota et al. (1989), the inverse U-shaped cavitation cloud contains a strong vortex cavitation at the center surrounded by many small cavitation bubbles (Fig. 1 (c)). Flowing downstream, the cavitation cloud begins to shrink because of the increase of static pressure along the chord. The vortex cavitation at the center also shrinks downstream. Finally, the cavitation cloud totally collapses at a certain point downstream.

Table 1. Experimental conditions and appearance of cavitation.

Cavitation No.	Observation Point		
	37% chord	52% chord	65% chord
σ =1.86	Shrinking from maximum volume	A few small vortex cavitations	No vortex cavitation
σ =1.72	Almost maximum of cavitation cloud	Shrinking	Small vortex cavitation still exists.
σ =1.61	(No Experiment)	Shrinking	Large vortex cavitation still exists.

Eight experimental conditions were selected to observe a wide aspect of the cavitation cloud. The experimental conditions are listed in Table 1 with a description of the corresponding cavitation appearance. The generation and collapse of the cavitation cloud were examined in detail before taking a hologram of the cavitation cloud. Figure 3 shows one cavitation cloud cycle observed from the top using a high-speed video. The experimental conditions were angle of attack: 8.4 deg, mean flow velocity: 8.0 m/s, and cavitation number: 1.72. The framing rate of the high-speed video was 4500 frames/sec.

The series of pictures shows every fourth frame, so that the interval between successive pictures is 0.89 ms. At t=0, the sheet cavitation extends from the leading edge until about 30% chord. About one-third of the sheet cavitation on the left begins to separate, which is clear on the pictures at t=0.89 ms and 1.78 ms. It becomes two U-shaped cavitation clouds, and flows downstream. The cavitation clouds become thinner and finally collapse around 60% chord position. (Not shown here.) During this process, a new sheet cavity grows and the same phenomena repeat periodically.

3. Laser Holography Setup and Calibration

Figure 4 shows the experimental setup for recording the hologram; this setup is basically the same as presented in the previous papers (Yamaguchi et al. 1990; Maeda et al. 1991). A ruby laser, NPG-60MPE (Nihon Kagaku Engineering Co. Ltd.), emits a single light pulse with 30~50 ns pulse length, 0.6943 μm wavelength and 300~500 mJ one-pulse energy. The holographic plate, 10E75 (Agfa Gvaert Co. Ltd.), has a resolution of 2,800 lines/mm. The laser beam is first divided into two beams. One beam, the object beam, goes into the tunnel through a ground glass plate. It becomes parallel beam of 30 mm in diameter through the concave and convex lenses. The position of the laser beam is illustrated in Fig. 5, where the center of the beam is at 65% chord. The light scattered by the bubbles in the cavitation cloud produces a real image in space, including the holographic plate through two convex lenses. The magnification ratio of the image is 5. The other beam, the reference beam, is guided below the tunnel test section and meets the holographic plate after it is expanded by the concave and convex lenses. The interference fringes of the object and reference beams are recorded on the holographic plate. The angle between the object and reference beams was determined as 44.5 deg. If the holographic plate is placed perpendicular to the object beam, the real image of the cavitation cloud is slightly disturbed by the weak beams reflected at the holographic plate and the convex lens in front of the plate. To avoid this, the holographic plate is inclined by 2.5 deg. The inclination of the holographic plate has made the reconstructed 3D holography image more distinct.

Figure 6 schematically illustrates the setup for reconstructing the holograms and analyzing the resulting 3D images. We cannot use the ruby laser for the reconstruction of the image, because it is a pulse laser. Instead, a He-Ne laser is used, which emits a continuous light beam with 0.6328 μm wavelength (approximately the same wavelength as the ruby laser). When a He-Ne laser beam is irradiated onto the hologram, the light diffracted by the interference fringes on the hologram reconstructs the real 3D image in the back of the hologram. The reconstructed image is scanned by a CCD TV camera mounted on an x-y-z stage which is controlled by a personal computer. The camera records a chordwise section of the image, which is the section perpendicular to the reconstructed image axis. The signal from the TV camera is sent to a personal computer through an A/D converter and converted to a digital picture of 512 × 512 elements with 8 bit (256) brightness levels. The bubble radii and positions are measured manually on the TV monitor screen, using the mouse of the personal computer. The image on the TV screen can be magnified by inserting various closeup rings to the TV camera. Magnification at this stage, however,

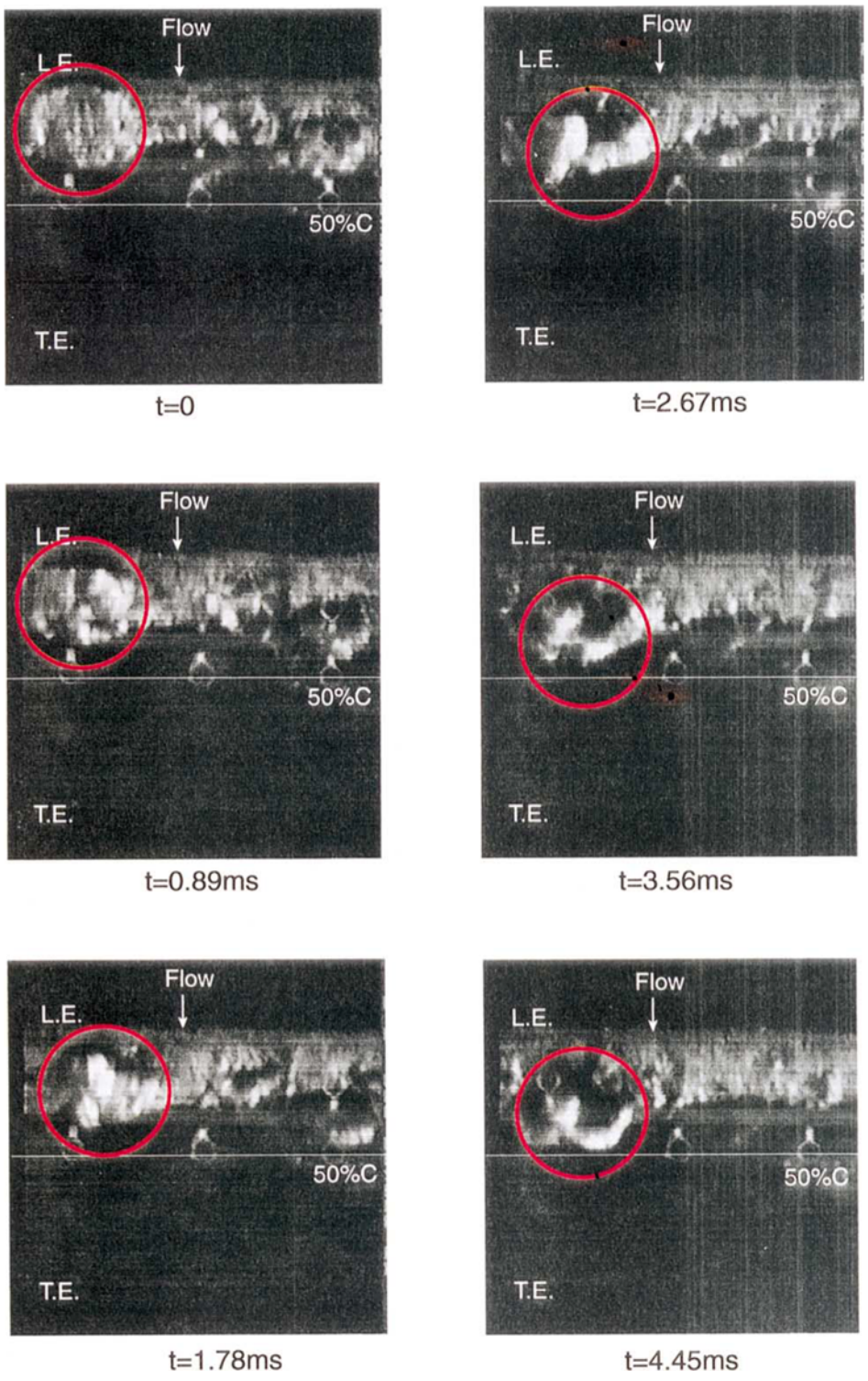

Fig. 3. One cycle of cavitation cloud development (σ =1.72, Time interval 0.89 ms).

also magnifies the noise. In order to measure the bubbles accurately, it is important to magnify the real image when recording the hologram, using the setups shown in Fig. 4.

The reference frame shown in Fig. 7 was placed on the model foil and recorded on a hologram to measure the magnification ratio of the reconstructed 3D holography image against the original. The diameter of the wires at both sides of the reference frame was measured with a microscope beforehand. Figure 8 shows the photographs of the TV monitor images which show the wires at both sides of the reference frame in the reconstructed 3D

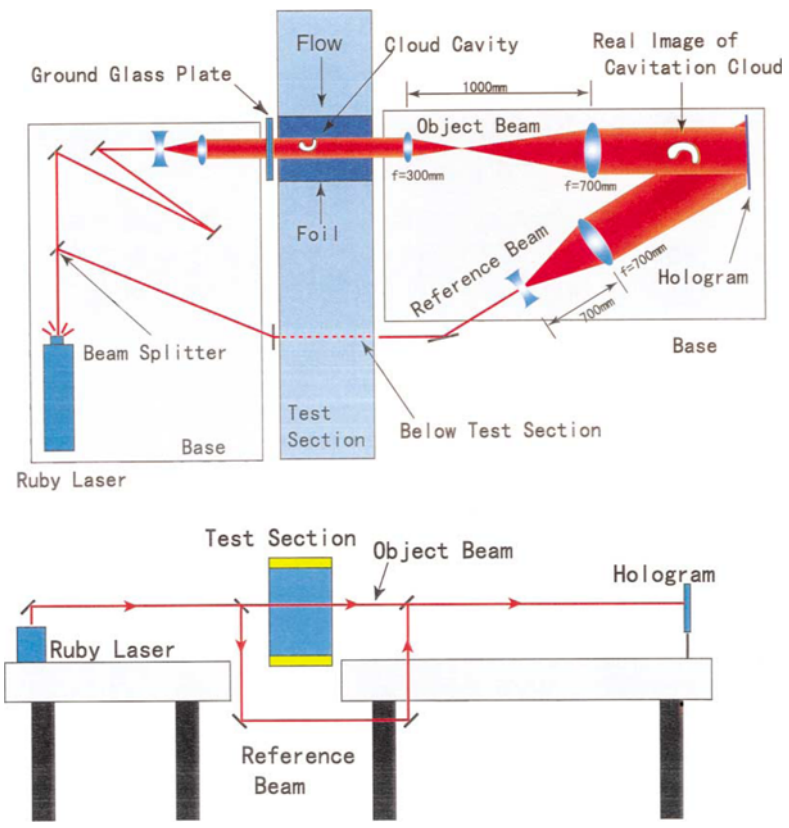

Fig. 4. Setup for recording the holograms.

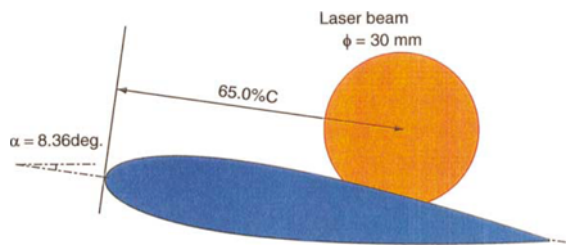

Fig. 5. Foil section (NACA0015) and laser beam.

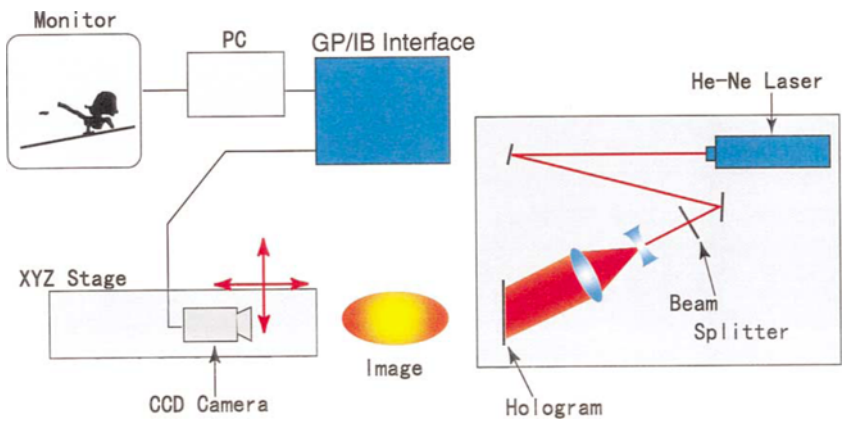

Fig. 6. Setup for reconstructing holograms and analyzing the 3D images.

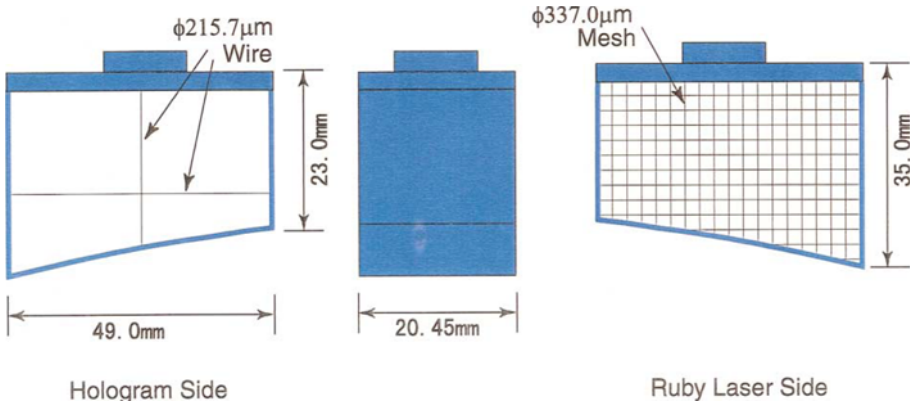

Fig. 7. Reference frame used for calibrating the reconstructed 3D holography image placed on the model foil.

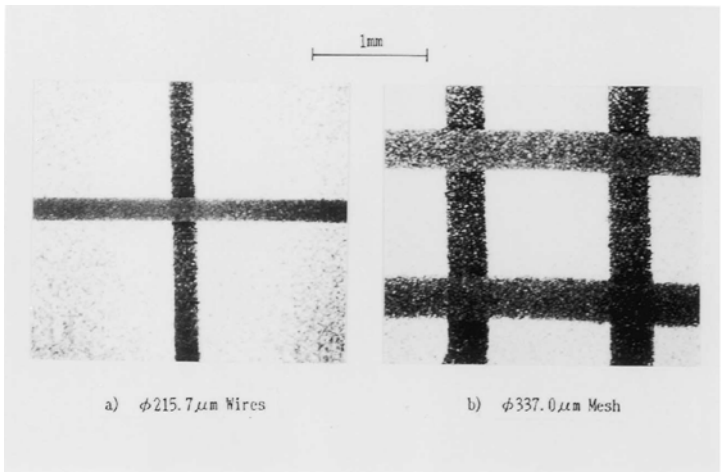

Fig. 8. TV monitor images of the reconstructed holograph of the reference frame wires.

holographic image. The width of the wires at both sides of the frame was used for the calibration of length in the chordwise and spanwise directions.

Although the magnification ratio can be calculated from the focal length of the lenses, the refractive index of the water and the wavelength of light, a slight error in adjusting the optical system sometimes results in a substantial discrepancy in the magnification ratio. Therefore, such the calibration is required in an off-axis laser holography system.

4. Reconstructed Images of Cavitation Cloud

Figure 9 shows the reconstructed image of a hologram taken at σ=1.86 and 37% chord, whereas Figure 10 shows a photograph of cavitation clouds taken from the top view at exactly the same time as Fig. 9. Figure 10 was taken with only a ruby laser light (red light) as it was emitted to record the hologram. Figure 11 is an illustration explaining the relationship between Figs. 9 and 10. The vortex cavitation is seen as a large dark mass on the reconstructed image of Fig. 9. The cavitation bubbles are also seen as small dark spots. Smaller bubbles are difficult to distinguish from speckle noise. The same vortex cavitation is shown as a bright red string in Fig. 10 (arrow in the figure). Many cavitation bubbles are also seen as small bright spots in the photograph. The major and the most important difference between the two figures is, of course, that the reconstructed holographic image is 3D, whereas the photograph (Fig. 10) is 2D.

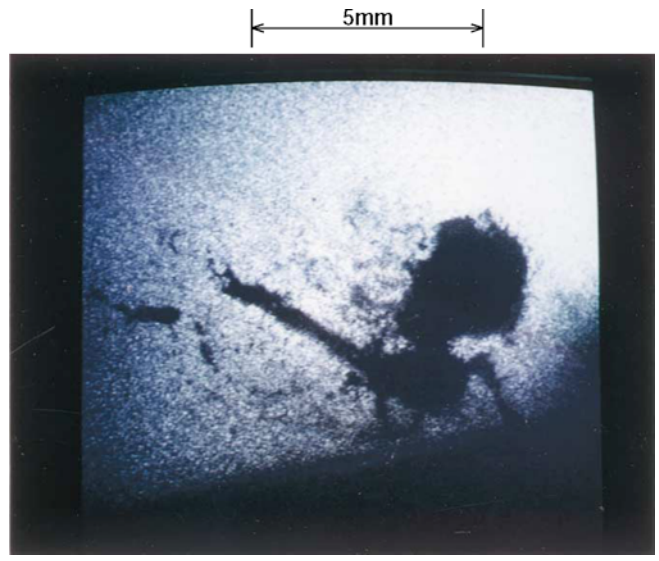

Fig. 9. Reconstructed image of hologram (σ =1.86 and 37% chord).

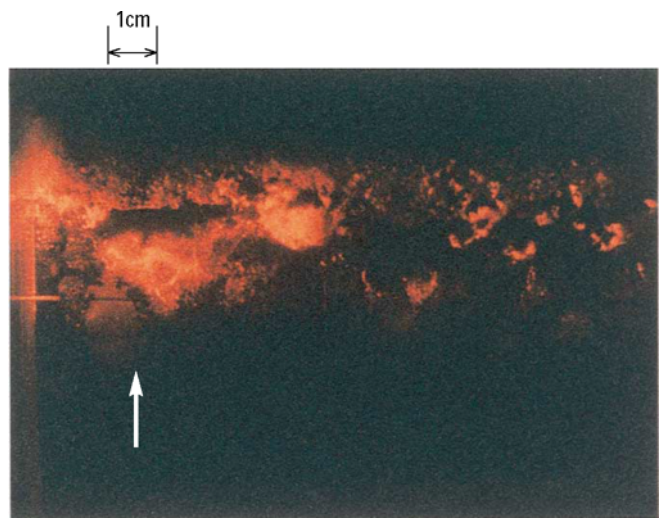

Fig. 10. Top view photograph of cavitation cloud taken at exactly the same time as Fig. 9.

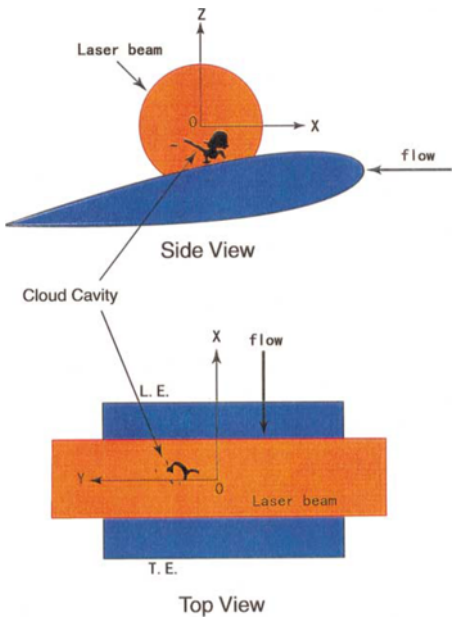

Fig. 11. Illustration to explain the relationship between Fig. 9 and Fig. 10.

By scanning the holographic image using a CCD TV camera on an x-y-z stage, the spatial distribution of the cavitation bubbles and vortex cavitation was measured. Smaller cavitation bubbles are more difficult to distinguish from speckle noise.

Moving the TV camera slightly into the y direction in Fig. 11, one can distinguish between speckle noise and the real image of bubbles on a TV screen. The human eyes are superior to the computer program in distinguishing real bubbles from speckle noise. The limit is about 10 μm in radius at the present case.

Figure 12 shows all the cavitation bubbles and vortex cavitations analyzed from the hologram shown in Fig. 9. The vortex cavitation is shown as a cluster of spheres whose diameters were drawn arbitrarily.

The spatial position of individual bubbles in the focal direction (y direction in Fig. 11) is determined by finding the focal position, a time-consuming and tiresome process, that also greatly reduces measurement accuracy. The estimated measurement accuracy is shown in Table 2.

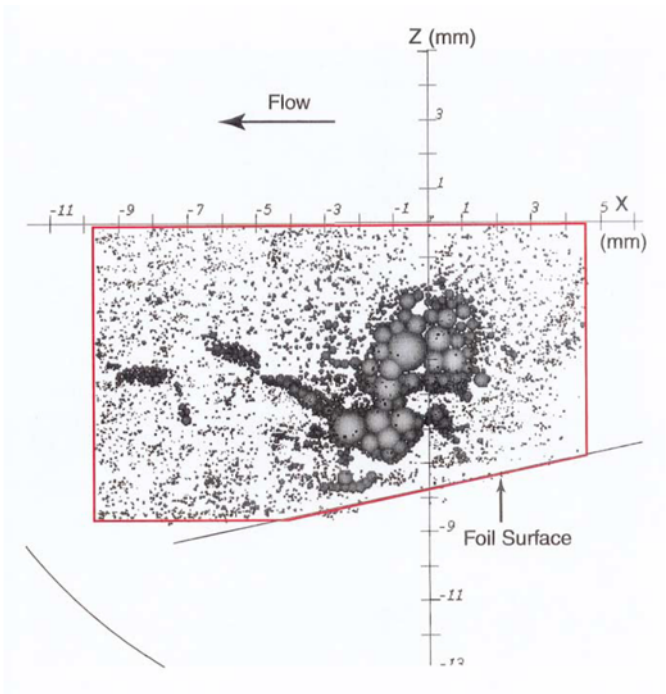

Fig. 12. Spatial distribution of cavitation bubbles and vortex cavitation at σ =1.86 and 37% chord (analyzed from hologram shown in Fig. 9).

Table 2. Accuracy of Measurement.

Items	Accuracy
Bubble diameter	±10 μm
Position of bubble	
In vertical plane to focal direction	±10 μm
Focal direction	±0.2 mm

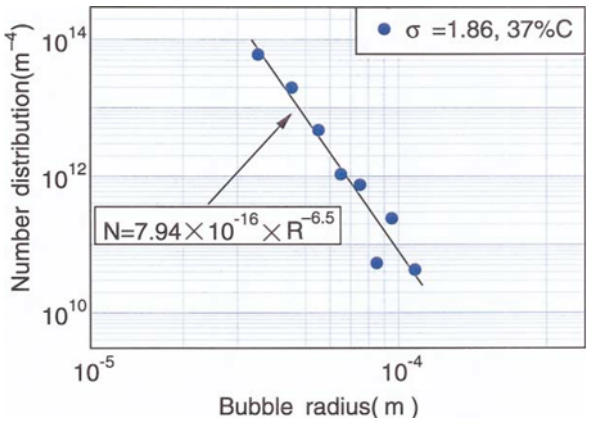

Fig. 13. Number distribution of cavitation bubbles at σ =1.86 and 37% chord.

In Fig.12 all 5106 cavitation bubbles (larger than 35 μm in radius) are shown; the examined volume is 3727 mm^3, thus the bubble density is 1370 bubbles/cm^3. The total working hour for the analysis of the reconstructed image was more than 100 hours. Figure 13 shows the number distribution of measured cavitation bubbles. There is a clear tendency for the bubbles to decrease in size. The empirical equation is also shown in the figure. The void ratio of the cavitation bubbles is only 0.02% when the vortex cavitation is not included.

Another set of measurements taken at σ =1.72 and at 52% chord is shown in Figs. 14-16. A pair of inverse U-shaped vortex cavitations are seen in the figures. The total number of bubbles larger than 35 μm in radius was 2958 in 5413 mm^3, which corresponds to 546 bubbles/cm^3. As expected, the cavitation bubbles do not exist uniformly in space. In many cases, large bubbles, which are more harmful than smaller ones, exist in a row. It strongly suggests that the vortex cavitation in a cavitation cloud collapses into large cavitation bubbles first. Then the bubbles collapse finally, that causes generation of a strong impulsive pressure peak. This observation is in agreement with the fact that erosion often occurs when one of the legs of a vortex cavitation touches and collapses on the solid surface.

Fig. 14. Reconstructed image of hologram (σ =1.72 and 52% chord).

Fig. 15. Top view photograph of cavitation cloud taken at exactly the same time as Fig.14.

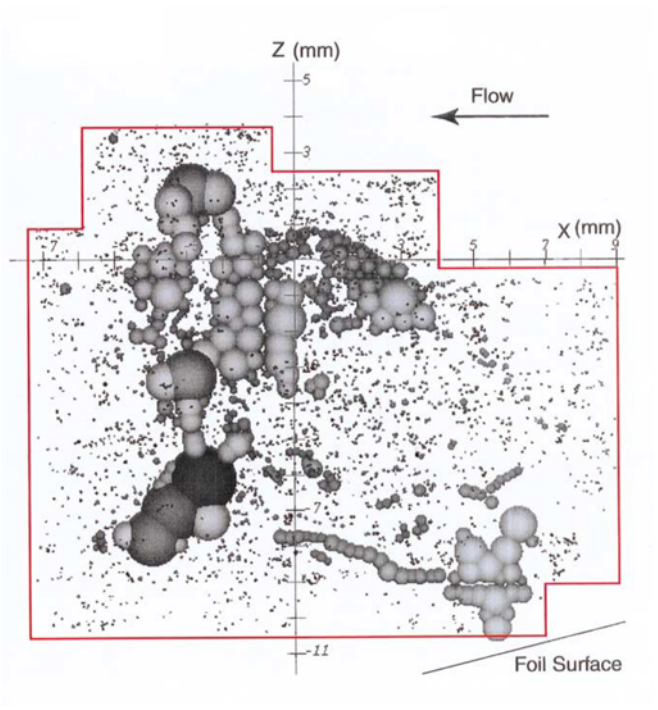

Fig. 16. Spatial distribution of cavitation bubbles and vortex cavitations at σ =1.72 and 52% chord (analyzed from hologram shown in Fig. 14).

5. Discussions

Figure 17 shows the summary of measured bubble number distribution for different cavitation numbers and also at different chord positions. In the figure, two previous values (σ =2.19, 60% chord by Kawanami et al., 1997 and σ =1.96, 60% chord by Maeda et al. 1991) are included.

Although the maximum number of bubbles with a certain radius is almost two orders of magnitude more than the minimum number case, the number distribution tendency is surprisingly similar in spite of the significant change in conditions. When the number distribution N (1/m^4) against bubble radius R (m) is expressed as

$$N = aR^{-n}, \tag{2}$$

the power n is between 3.8 and 6.5, except for one extreme case (σ =1.72, 65% chord), where n=17.3. Under this condition, the cavitation cloud had already collapsed and a relatively small number (1104 bubbles in 3263 mm^3) of bubbles were observed.

The authors tentatively propose the empirical equation

$$N = aR^{-5.1} \tag{3}$$

for the bubble number distribution function in a cavitation cloud. Such a distribution function is useful for realistic modelling of the numerical analysis of a cavitation cloud.

Yu and Ceccio (1997) made a similar measurement downstream of a stable partial cavity. They observed gas bubbles (not cavitation bubbles) far downstream of partial cavity, because their aim was to determine the diffusion rate of noncondensable gas into the partial cavity. According to their measurement, the bubble number distribution was greatly affected by the gas content dissolved in water. Nevertheless, the exponent in Eq. (2) was between 5 and 6 in the range of bubbles larger than 100 μm in radius, which agrees with our results.

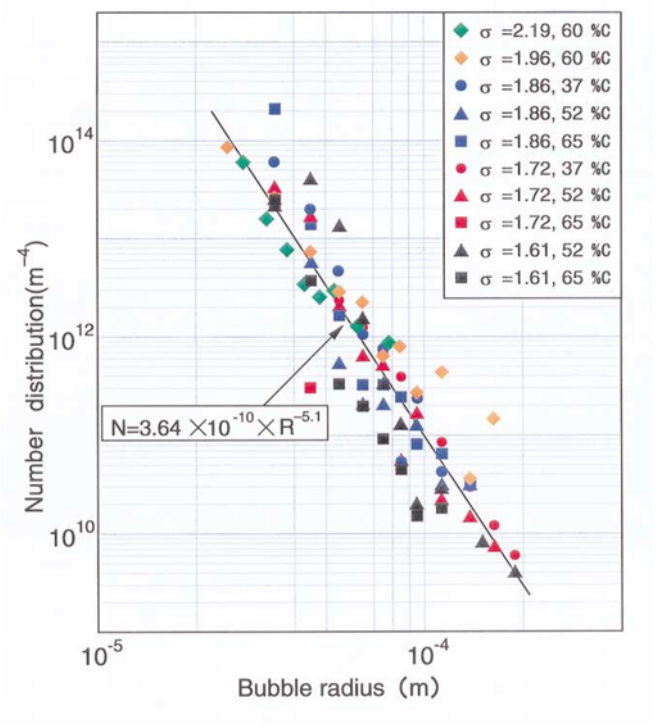

Fig. 17. Bubble number distribution in cavitation cloud under various conditions.

6. Conclusions

Bubble distributions in the cavitation cloud downstream of a sheet cavitation were measured with an off-axis laser holography system. This system can measure bubbles larger than 10 μm in radius. The measurement was, however, mainly concentrated on bubbles larger than 35 μm in radius, because larger bubbles are more harmful as a source of impulsive high pressure. The bubble density (larger than 35 μm) was on the order of 10^3 bubbles/cm^3.

The present observation provided spatial information on the vortex cavitation and bubbles in a cavitation cloud. The vortex cavity was an inverse U shape whose two legs touched the foil surface. The inverse U shape inclined towards the foil surface. It is considered that the inverse U-shaped vortex cavitation is the essential flow structure of a cavitation cloud.

The bubble number distribution N (1/m^4) can be expressed as a power function of bubble radius R (m) for large bubbles:

$$N = aR^{-n},$$

The power n is about 5 in the present experiment.

References

Acosta, A., O'Hern, T., and Katz, J., Some Recent Trends in Cavitation Research, Proceedings of Int. Symp. on Cavitation, Sendai, Japan, 1-7, (1986).

Avellan, F., Dupont, P., and Ryhming, I., Generation Mechanism and Dynamics of Cavitation Vortices Downstream of a Fixed Leading Edge Cavity, Proc. 17th Symp. on Naval Hydrodynamics, 317-329, (1988).

Billet, M.L., Cavitation Nuclei Measurements with an Optical System, J. Fluids Eng. ASME, Vol. 108, No. 3, 366-372, (1986).

Brennen, C.E., Cavitation and Bubble Dynamics, Oxford Eng. Science Series, Oxford Univ. Press, (1995).

Brennen, C.E., Colonius, T., and d'Auria, F., Computing Shock Waves in Cloud Cavitation, Proc. 3rd Int. Symp. on Cavitation, Grenoble, France, Vol. 2, 287-294, (1998).

Chahine, G.L., Cloud Cavitation: Theory, Proc. 14th Symp. on Naval Hydrodynamics, Washington D.C., U.S.A., 165-194, (1983).

de Lange, D.F., de Bruin, G.J., and van Wijnngaarden, L., On the Mechanism of Cloud Cavitation-Experiment and Modelling, Proc. 2nd Int. Symp. on Cavitation, Tokyo, Japan, 45-49, (1994).

Fortes-Patella, R. and Reboud, J.L., A New Approach to Evaluate the Cavitation Erosion Power, Proc. Int. Symp. on Cavitation, CAV'95, Deauville, France, 233-240, (1995).

Hammitt, F.G., Cavitation and Multiphase Flow Phenomena, McGraw-Hill Inc., (1980).

Kato, H., Advances in Marine Hydrodynamics (Ed. Ohkusu M.) Chap. 5 Cavitation, Computational Mechanics Publications, 233-277, (1996).

Kawanami, Y., Kato, H., Yamaguchi, H., Tanimura, M., and Tagaya, Y., Mechanism and Control of Cloud Cavitation, J. Fluids Eng. ASME, Vol. 119, No. 4, 788-795, (1997).

Kawanami, Y., Kato, H., and Yamaguchi, H., Three-Dimensional Characteristics of the Cavities Formed on a Two-Dimensional Hydrofoil, Proceedings of the Third Int. Symp. on Cavitation, France, Vol. 1, 221-226, (1998).

Knapp, R.T., Recent Investigations of the Mechanics of Cavitation and Cavitation Damage, Trans. ASME, Vol. 77, 1045-1054, (1955).

Knapp, R.T., Daily, J.W., and Hammit, F.G., Cavitation, McGraw-Hill Book Co., (1970).

Konno, A., Kato, H., Yamaguchi, H., and Maeda, M., Observation of Cavitation Bubble Collapse by High-Speed Video, Proc. 5th Asian Symp. on Visualization, Bali, Indonesia, (1999).

Kubota, A., Kato, H., Yamaguchi, H., and Maeda, M., Unsteady Structure Measurement of Cloud Cavitation on a Foil Section using Conditional Sampling Technique, J. Fluids Eng. ASME, Vol. 111, 204-210, (1989).

Maeda, M., Yamaguchi, H., and Kato, H., Laser Holography Measurement of Bubble Population in Cavitation Cloud on a Foil Section, ASME, FED-Vol. 116, (1991), Cavitation '91, 67-76.

Matsumoto, Y., Bubble Dynamics in Cavitation, Proc. 3rd Int. Symp. on Cavitation, Grenoble, France, Vol. 1, 3-8, (1998).

Mørch, K.A., Cavity Cluster Dynamics and Cavitation Erosion, Cavitation and Polyphase Flow Forum-1981, ASME, 1-10, (1981).

Reisman, G.E. and Brennen, C.E., Pressure Pulses Generated by Cloud Cavitation, Symp. on Cavitation and Gas-Liquid Flows in Fluid Machinery and Devices, ASME, FED-236, 319-328, (1996).

Shen, Y.T. and Peterson, F.B., Unsteady Cavitation on an Oscillating Hydrofoil, Proc. 12th Symp. on Naval Hydrodynamics, 32-384, (1978).

Takahira, H., Akamatsu, T., and Fujikawa, T., Dynamics of a Cluster of Bubbles in a Liquid (Theoretical Analysis), JSME Int. J. Series B, Vol. 37, 297-305, (1994).

van Wijngaarden, L., On the Collective Collapse of a Large Number of Gas Bubbles in Water, Proc. 11th Int. Congress of Applied Mechanics, Munich, Germany, 854-861, (1964).

Wang, Y.-C. and Brennen, C.E., Shock Wave Development on the Collapse of a Cloud Bubbles, Cavitation and Multiphase Flow Forum, ASME, FED-194, 15-19, (1994).

Yamaguchi, H., Kato, H., Kamijo, A., and Maeda, M., Development of a Laser Holography System for the Measurement of Cavitation Bubble Clusters, Cavitation and Multiphase Flow Forum, ASME, FED-Vol. 98, Toronto, Canada, 115-119, (1990).

Young, F.R., Cavitation, McGraw-Hill Book Co., (1989).

Yu, P.-W. and Ceccio, S.L., Diffusion Induced Bubble Populations Downstream of a Partial Cavity, J. Fluids Eng. ASME, Vol. 119, 782-787, (1997).

Authors' Profiles

Hiroharu Kato: He received his B. Eng. degree in naval architecture in 1961, and his PhD in mechanical engineering in 1966 both from the University of Tokyo. He has been a professor at the Department of Environmental and Ocean Engineering, University of Tokyo until March 1999. Presently a professor at the Mechanical Engineering Department, Toyo University. He was the president of the Visualization Society of Japan in 1997-1998. His major research field is cavitation, turbulent drag reduction, heat transfer, and environmental engineering.

Hajime Yamaguchi: He received his PhD degree in naval architecture in 1983 from the University of Tokyo. He works at the Department of Environmental and Ocean Engineering, the University of Tokyo as an associate professor. His research interest is polar environmemtal engineering and cavitation.

Masatsugu Maeda: He is a research associate at the Department of Environmental and Ocean Engineering, the University of Tokyo. He has been working on cavitation tunnel experiment for 30 years.

Y. Kawanami: He received a bachelor and a master degree both in engineering from the University of Tokyo. He works for the Ship Research Institute as a research fellow.

Shogo Nakasumi: He graduated Dept. of Naval Architecture and Ocean Engineering, the University of Tokyo in 1998. Presently a master-course student, Dept. of Environmental and Ocean Engineering, the University of Tokyo.